Journal of Turbulence

ISSN: (Print) 1468-5248 (Online) Journal homepage: http://www.tandfonline.com/loi/tjot20

Two-equation hybrid RANS–LES models: a novel way to treat k and ω at inlets and at embedded interfaces

L. Davidson

To cite this article: L. Davidson (2017) Two-equation hybrid RANS–LES models: a novel way to treat k and ω at inlets and at embedded interfaces, Journal of Turbulence, 18:4, 291-315, DOI: 10.1080/14685248.2017.1281417

To link to this article: http://dx.doi.org/10.1080/14685248.2017.1281417

JOURNAL OF TURBULENCE, 2017
VOL. 18, NO. 4, 291–315
http://dx.doi.org/10.1080/14685248.2017.1281417

Taylor & Francis
Taylor & Francis Group

Two-equation hybrid RANS–LES models: a novel way to treat k and ω at inlets and at embedded interfaces

L. Davidson

Division of Fluid Dynamics, Department of Applied Mechanics, Chalmers University of Technology, Gothenburg, Sweden

ABSTRACT

A novel method for prescribing k and ω at inlets and RANS–LES interfaces in embedded LES is presented and evaluated. The method is based on the proposal by Hamba to use commutation terms at RANS–LES interfaces. Commutation terms are added to the k and ω equations in the region near the inlet (i.e. the RANS–LES interface). The proposed method can also be used when prescribing inlet values for k and ω in hybrid LES–RANS. The commutation terms are added in embedded LES at the LES side of the RANS–LES interface. The influence of the extent of the region where the commutation terms are added is investigated. It is found that it is most efficient to add commutation terms in only one cell layer adjacent to the interface; in this way, tuned constants are avoided. The commutation term in the ω equation is derived from transformation of the k and ε equations. When the commutation terms are used in only one cell layer, the commutation term in the k equation corresponds to a negative convection term. Hence, the commutation term can be omitted and a homogeneous Neumann inlet boundary condition can be used. The commutation term in the ω equation is retained. The novel method is evaluated for channel flow ($Re_\tau = 8000$), boundary layer flow ($Re_\theta = 11,000$) and backward-facing step flow ($Re_H = 28,000$). Hybrid LES–RANS is used for the first two flows and embedded LES for the backward-facing step flow.

ARTICLE HISTORY
Received 15 March 2016
Accepted 4 January 2017

KEYWORDS
LES; commutation term; embedded LES; hybrid RANS–LES; RANS–LES interface condition; LES inlet conditions

1. Introduction

In embedded LES, part of the flow is treated by RANS and part by LES. We are interested in the present work in a configuration where the upstream region is treated by RANS and the downstream by LES, and the interface is vertical, parallel to the inlet. We denote the interface between the two regions as 'the RANS–LES interface' located at x_{R-L}. The transition region in which the predicted flow is in-between RANS and LES is often called the *grey area*, a problem described in [1]. When the flow goes from a RANS region to an LES region through the RANS–LES interface, it should – in order to minimise the grey area – switch as quickly as possible from RANS mode to LES mode.

Chauvet et al. [2,3] find that the standard DES model predicts the transition to turbulent flow in a round jet too late. As a remedy, they propose a new way to define the turbulent

CONTACT L. Davidson lada@chalmers.se

length scale, Δ, using the vorticity. The length scale is defined by the length of the cell area normal to the vorticity. This gives a reduced $\Delta \simeq \sqrt{\Delta x \Delta y}$ for a 2D shear layer in the x–y plane, which promotes transition to full LES.

In order to trigger shear-layer instabilities in a shear layer, Kok and van der Ven [4] use a stochastic SGS model in combination with a high-pass filter of the velocity gradient used in the SGS model. The high-pass filter ensures that the mean flow gradients are excluded when computing the velocity gradients in the production terms in the k and ω equations. This means that, when the flow is steady, no SGS turbulence is generated, which reduces damping of unsteadiness and promotes the growth of shear-layer instabilities.

Mockett et al. [5] propose a third way to achieve reduced turbulent viscosity. They modify the expression for the symmetric strain-rate tensor, $\bar{s}_{ij}$, which appears in the Smagorinsky model (which corresponds to a DDES model in LES mode). They evaluate two different expressions for the symmetric strain-rate tensor, that in the WALE model [6] and that in the σ model [7]. They combine this approach with a novel way for the turbulent length scale. They use the vorticity – as in [2,3] – and their formulation gives, for a 2D shear layer, a turbulent length scale $\Delta \simeq ((\Delta x)^2 + (\Delta y)^2)^{1/2}/\sqrt{3}$. They find that the strain-rate from the σ model together with the proposed new turbulent length scale is superior to using the strain-rate from the WALE model. Shur et al. [8] evaluate this formulation of Δ in more detail and confirm that this choice of length scale is suitable.

Girimaji and Wallin [9] use the PANS (partially averaged Navier–Stokes) $k-\varepsilon$ model, which is based on f_k. It is defined as the ratio of modelled to total (i.e. modelled plus resolved) turbulence. In a RANS region $f_k = 1$ and in an LES region, f_k should go towards zero (the better the resolution, the smaller f_k). When the grid is non-uniform, a commutation error appears because the filtering and the spatial derivative do not commute. To account for the non-uniform mesh, Girimaji and Wallin [9] derived an additional commutation term to be added in the k equation. Later, Davidson [10] extended this methodology to RANS–LES interfaces across which there is a strong gradient of the turbulent length scale. He showed that adding a commutation term in the k equation at a RANS–LES interface – inlet or embedded LES (interface parallel to the inlet) or hybrid LES–RANS (interface parallel to a wall) – gives a strongly reduced k in the LES region adjacent to the RANS–LES interface; as a consequence, the turbulent viscosity is also reduced.

Davidson [11] uses the scale-similarity model to create backscatter and produce resolved turbulence in order to mitigate the grey area problem. The original scale-similarity model of Bardina et al. [12] is known to give too little SGS dissipation. In [11], it is formulated in such a way that it can be strictly dissipative or non-dissipative (i.e. only backscatter). Peng [13] also proposes a model based on the scale-similarity stresses, but here it is formulated as an additional Leonard term, which gives backscatter and thereby stimulates the growth of resolved turbulence.

Hamba [14] showed that, when the filter size (i.e. the grid) is non-uniform, a commutation error appears in SGS models based on transport equations. He found by analyzing DNS channel data that this commutation term is large at interfaces between RANS and LES. In the present work, the commutation term derived in [14] is used at RANS–LES interfaces. The two-equation zonal $k-\omega$ hybrid RANS–LES model of Arvidson et al. [15] is employed. For channel flow and boundary layer flow, the commutation terms are used adjacent to the inlet, which is treated as a RANS–LES interface. RANS inlet values are prescribed for k and ω. In the third test case, embedded LES is used to simulate the backward-facing step.

The commutation terms are added in the LES region adjacent to the RANS–LES interface located near (or at) the step.

The paper is organised as follows. The two-equation zonal $k-\omega$ hybrid RANS–LES model is first presented. The commutation terms are then introduced and formulated, and a short description of the numerical method is given. A description of the procedure for generating synthetic fluctuations (used at the inlet and the embedded RANS–LES interface) follows. The results are presented in the next section where the effect of the commutation terms is evaluated. Some conclusions are drawn in the final section.

2. The zonal k–ω hybrid RANS–LES model

In the LES region, the model reads

$$\frac{\partial k}{\partial t}+\frac{\partial \bar{v}_i k}{\partial x_i}=P^k-f_k\frac{k^{3/2}}{\ell_t}+\frac{\partial}{\partial x_j}\left[\left(\nu+\frac{\nu_t}{\sigma_k}\right)\frac{\partial k}{\partial x_j}\right], \tag{1}$$

$$\frac{\partial \omega}{\partial t}+\frac{\partial \bar{v}_i \omega}{\partial x_i}=C_{\omega_1}f_\omega\frac{\omega}{k}P^k-C_{\omega 2}\omega^2+\frac{\partial}{\partial x_j}\left[\left(\nu+\frac{\nu_t}{\sigma_\omega}\right)\frac{\partial \omega}{\partial x_j}\right]+C_\omega\frac{\nu_t}{k}\frac{\partial k}{\partial x_j}\frac{\partial \omega}{\partial x_j}, \tag{2}$$

$$\nu_t=f_\mu\frac{k}{\omega},\quad P^k=\nu_t\left(\frac{\partial \bar{u}_i}{\partial x_j}+\frac{\partial \bar{u}_j}{\partial x_i}\right)\frac{\partial \bar{u}_i}{\partial x_j},\quad \ell_t=\Psi_{PDH}C_{LES}\Delta_{dw},$$

$$\Psi_{PDH}=\min\left[10,\ f_k\left(\frac{f_\omega}{f_\mu}\right)^{3/4}\right],\quad \Delta_{\max}=\max\{\Delta x,\ \Delta y,\ \Delta z\},$$

$$\Delta_{dw}=\min\left(\max\left[C_{dw}d_w,\ C_w\Delta_{\max},\ \Delta_{nstep}\right],\ \Delta_{\max}\right), \tag{3}$$

where d_w denotes the distance to the nearest wall and Δ_{step} is the grid step size in the wall-normal direction. The damping functions read

$$f_k=1-0.722\cdot\exp\left[-\left(\frac{R_t}{10}\right)^4\right],\quad f_\omega=1+4.3\cdot\exp\left[-\left(\frac{R_t}{1.5}\right)^{1/2}\right],$$

$$f_\mu=0.025+\left\{1-\exp\left[-\left(\frac{R_t}{10}\right)^{3/4}\right]\right\}\left\{0.975+\frac{0.001}{R_t}\cdot\exp\left[-\left(\frac{R_t}{200}\right)^2\right]\right\}.$$

The turbulent Reynolds number is defined as $R_t=k/(\nu\omega)$. The length scale, Δ_{dw}, is taken from the IDDES model [16]. In the RANS regions, $\ell_t=k^{1/2}/(C_k\omega)$. The constants read $\sigma_k=0.8$, $\sigma_w=1.35$, $C_k=0.09$,$C_{\omega 1}=0.42$, $C_{\omega 2}=0.075$, $C_\omega=0.75$, $C_{LES}=0.7$ and $C_{dw}=0.15$. Details on the zonal k–ω hybrid RANS–LES model can be found in [15].

The difference between Equations (1) and (2) in the RANS and LES regions can be summarised as follows: in RANS regions, the RANS length scale, $\ell_t=k^{1/2}/(C_k\omega)$, is used in the dissipation term in the k equation and, in LES regions, the filter length scale, Δ_{dw}, is used.

3. Commutation terms in the k and ω equations

When the filter size in LES varies in space, an additional term appears in the momentum equation because the spatial derivatives and the filtering do not commute. For the convective term in Navier–Stokes, for example, we get

$$\overline{\frac{\partial v_i v_j}{\partial x_j}} = \frac{\partial}{\partial x_j}(\overline{v_i v_j}) + \mathcal{O}\left((\Delta x)^2\right).$$

Ghosal and Moin [17] show that the error is proportional to $(\Delta x)^2$ and, since this error is of the same order as the discretisation error of most finite volume methods, it is usually neglected.

However, in zonal hybrid (by "zonal", we imply that the interface is chosen at a location where the RANS and LES length scales differ) RANS–LES, the length scale at the RANS–LES interface changes abruptly from a RANS length scale to an LES length scale. Hamba [14] estimated the commutation error at RANS–LES interfaces and found that it is large. The commutation term for the divergence of a flux, q_i, reads

$$\overline{\frac{\partial q_i}{\partial x_i}} = \frac{\partial \bar{q}_i}{\partial x_i} - \frac{\partial \Delta}{\partial x_i}\frac{\partial \bar{q}_i}{\partial \Delta}$$

For the k equation, the commutation term reads [14]

$$\overline{\frac{\partial u_i k}{\partial x_i}} = \frac{\partial \bar{u}_i k}{\partial x_i} - \frac{\partial \Delta}{\partial x_i}\frac{\partial \bar{u}_i k}{\partial \Delta}. \tag{4}$$

Consider a fluid particle in a RANS region moving in the x_1 direction and passing across a RANS–LES interface. The filter width decreases across the interface, i.e.

$$\frac{\partial \Delta}{\partial x_1} \simeq \frac{\Delta_{LES} - \Delta_{RANS}}{\Delta x_1} < 0 \tag{5}$$

and (note that k_{LES} is an estimated LES value of k, see Equation (11))

$$\frac{\partial \bar{u}_1 k}{\partial \Delta} \simeq \frac{u_1 k_{LES} - u_1 k_{RANS}}{\Delta_{LES} - \Delta_{RANS}} > 0 \tag{6}$$

which means that the last term on the right-hand side of Equation (4) gives a positive contribution on the left side of the k equation (Equation (1)); on the right side of Equation (1), it gives a negative contribution. Hence, the additional term in Equation (4) at a RANS–LES interface reduces k, as expected. To obtain the right-hand side of Equations (5) and (6), the derivatives on the left side of the equations have been estimated by simple finite-difference expressions, i.e.

$$\frac{df}{dx} \simeq \frac{\Delta f}{\Delta x}. \tag{7}$$

It may be noted that the idea of adding an additional source term in the k equation due to a commutation error is similar to the proposal of Girimaji and Wallin [9]; they use a commutation term based on the gradient of f_k in the PANS model. This idea was later used by the present author at RANS–LES interfaces [10].

To find the corresponding term in the ω equation, let us start by looking at the ε equation. What happens with ε when a fluid particle moves from a RANS region into an LES region? The answer is, nothing. The dissipation is the same in a RANS region as in an LES region. This is best seen by looking at the k_{sgs} equation

$$\frac{\partial k_{sgs}}{\partial t}+\frac{\partial \bar{v}_i k_{sgs}}{\partial x_i}=P^{k_{sgs}}+\frac{\partial}{\partial x_j}\left[\left(\nu+\frac{\nu_{sgs}}{\sigma_k}\right)\frac{\partial k_{sgs}}{\partial x_j}\right]-\varepsilon. \tag{8}$$

The dissipation term, ε, in Equation (8) is the same as the dissipation term in Equation (1) unless the resolution is very fine (close to DNS). Then, much of the dissipation is resolved, reducing the production term, $P^{k_{sgs}}$. However, this kind of resolution is not realistic.

Now consider the ω equation. It is derived by transformation of the k and ε equations to an ω equation as

$$\frac{d\omega}{dt}=\frac{d}{dt}\left(\frac{\varepsilon}{C_k k}\right)=\frac{1}{C_k k}\frac{d\varepsilon}{dt}+\frac{\varepsilon}{C_k}\frac{d(1/k)}{dt}=\frac{1}{C_k k}\frac{d\varepsilon}{dt}-\frac{\omega}{k}\frac{dk}{dt}. \tag{9}$$

The right-hand side shows that the source terms in the ω equation correspond to those in the ε equation multiplied by $1/(C_k k)$ together with those in the k equation multiplied by $-\omega/k$. Hence, the source term due to the commutation error in the ω equation is the commutation term in Equation (4) multiplied by $-\omega/k$ so that

$$\overline{\frac{\partial u_i \omega}{\partial x_i}}=\frac{\partial \bar{u}_i\omega}{\partial x_i}-\frac{\partial \Delta}{\partial x_i}\frac{\partial \bar{u}_i\omega}{\partial \Delta}=\frac{\partial \bar{u}_i\omega}{\partial x_i}+\frac{\omega}{k}\frac{\partial \Delta}{\partial x_i}\frac{\partial \bar{u}_i k}{\partial \Delta}. \tag{10}$$

Assuming again a flow in the x_1 direction from a RANS region to an LES region, we find that the second term on the right-hand side of Equation (10) is negative since $\partial\Delta/\partial x_1<0$ (see Equation (5)) and $\partial \bar{u}_1 k/\partial\Delta>0$ (see Equation (6)) so that the commutation term in Equation (10) is positive/negative on the right/left side of the ω equation (Equation (2)). This means that the commutation term in Equation (10) will increase ω when moving from a RANS region to an LES region. Hence, the source terms in the k and ω equations both contribute to reducing the turbulent viscosity, which is an effect we are looking for at RANS–LES interfaces: a reduced turbulent viscosity will promote growth of resolved turbulence on the LES side of an interface.

The commutation terms in Equations (4) and (10) are added in the transition region, $0<x-x_{R-L}<x_{tr}$ (see Figures 1 and 2); for the k equation, it is discretised as follows:

$$\begin{aligned}P^{k,c}=\left.\frac{\partial\Delta}{\partial x_1}\frac{\partial \bar{u}_1 k}{\partial\Delta}\right|_x&=\zeta\left(\frac{\Delta_{LES}-\Delta_{RANS}}{x_{tr}}\right)\left(\frac{\bar{u}_1 k_{RANS,x}-\bar{u}_1 k_{LES}}{\Delta_{RANS}-\Delta_{LES}}\right)\\&=\zeta\,\bar{u}_1\frac{k_{LES}-k_{RANS,x}}{x_{tr}},\quad \zeta=\frac{x-x_{R-L}}{x_{tr}},\end{aligned} \tag{11}$$

$$k_{LES}=\left(\frac{\nu_{sgs}}{\Delta}\right)^2,\quad \nu_{sgs}=(C_s\Delta)^2\,|\bar{s}|,\quad \Delta=(\Delta V)^{1/3},\quad C_s=0.1,$$

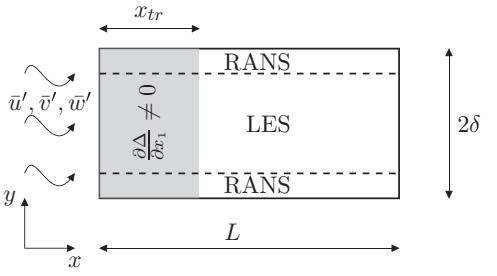

Figure 1. Channel flow.

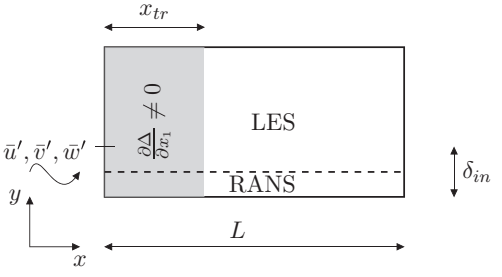

Figure 2. Boundary layer flow.

where k_{LES} is evaluated in the LES region, x_{R-L} denotes the location of the RANS–LES interface and x_{tr} is the extent of the transition region. If the commutation term is used only in the grid plane adjacent to RANS–LES interface, then $\zeta = 1$. Otherwise, it decreases from one at the interface plane to zero at $x - x_{R-L} = x_{tr}$. It may at first seem surprising that the final expression for $P^{k,c}$ does not include Δ. However, since it is assumed that Δ varies linearly with x, Δ in the nominator and denominator cancel. The filter width Δ does appear implicitly since k is assumed to go from k_{RANS} to k_{LES}, which depends on Δ_{RANS} and Δ_{LES}, respectively, over the distance x_{tr}. As mentioned above, the commutation terms are added in the region $0 \leq x - x_{R-L} \leq x_{tr}$ (see Figures 1 and 2), where $x_{R-L} = 0$ for the channel flow and the boundary-layer flow; for the backward-facing-step flow, $x_{R-L} = -H$ or $x_{R-L} = 0$.

It is found in Section 6 that it is not important where in the LES region k_{LES} is evaluated (k_{LES} is negligible compared to k_{RANS}). Initially, k_{RANS} was evaluated in the RANS region (in the channel flow and the boundary-layer simulations, the RANS region corresponds to an inlet), but that gives too large a gradient, and the simulations diverge. Instead, k_{RANS} is evaluated at the local x station (denoted by $k_{RANS,x}$) in the transition region. This ensures that the magnitude of the commutation term decreases smoothly from the start to the end of the transition region.

It may be argued that the commutation terms should formally be added only in the LES region and not in the RANS regions near the walls (see Figures 1 and 2). There is no physical reason to add the commutation terms in the RANS region because of the different formalism of the RANS and LES equations(see e.g. [18]). The argument for also adding a commutation term in the URANS region is that the turbulent viscosity (and the turbulent length scale) is much smaller in URANS than in RANS. This is clearly seen in fully

developed channel flow using hybrid LES–RANS models, where the turbulent viscosity in the URANS regions is much smaller than in pure RANS simulations (see, e.g. Figure 8(a) in [19]). Figure 8 shows that this is also true for the turbulent length scale. Hence, we choose to add commutation terms in the RANS regions as well in order to reduce the turbulent viscosity. In the baseline method, Equation (11) is also used in the URANS region. This method is used unless otherwise stated.

As an alternative, k_{LES} in Equation (11) may be replaced in the RANS regions with k_{URANS}, where k_{URANS} denotes the modelled turbulence kinetic energy in the unsteady RANS region. Taking guidance from hybrid LES–RANS of fully developed channel flow (Figure 8(a) in [19]), k_{URANS} is computed as

$$k_{URANS} = \begin{cases} k_{RANS} & y < y_{peak} \\ k_{peak} - (k_{peak} - k_{LES})\eta & y_{peak} < y < y_{int}, \end{cases} \tag{12}$$

where $\eta = (y - y_{peak})/(y_{int} - y_{peak})$; subscript *peak* denotes the peak value of k_{RANS} (i.e. of the RANS inlet profile) and subscript *int* is the location of the interface. The second line in Equation (12) makes k_{URANS} decrease linearly from the peak value at $y = y_{peak}$ to k_{LES} at $y = y_{int}$. The influence of different treatments of k_{URANS} in channel flow is presented below (see Figure 7).

4. Numerical method

An incompressible, finite-volume code is used [20]. The convective terms in the momentum equations are discretised using central differencing. Hybrid central/upwind is used for the k and ω equations. The Crank–Nicolson scheme is used for time discretisation of all equations. The numerical procedure is based on an implicit, fractional step technique with a multigrid pressure Poisson solver [21] and a non-staggered grid arrangement.

5. Synthetic fluctuations

In order to quickly create turbulence-resolved flow near the inlet boundary, turbulent fluctuations must be superimposed on the mean flow. Anisotropic synthetic fluctuations are used at the inlet for the channel flow and the boundary-layer flow and at the RANS–LES interface in the backward-facing flow. The methodology used in [22,23] is somewhat extended and involves the following steps:

(1) A pre-cursor RANS simulation (1D for the channel flow and 2D for the boundary-layer flow) is made using the PDH model [24].
(2) After having carried out the pre-cursor RANS simulation, the Reynolds stress tensor is computed using the EARSM model [25].
(3) The Reynolds stress tensor is used as input for generating the anisotropic synthetic fluctuations. The integral length scale is set to 0.3δ.
(4) Since the method of synthetic turbulence fluctuations assumes homogeneous turbulence, we can only use the Reynolds stress tensor in one point. We need to choose a relevant location for the Reynolds stress tensor. In a turbulent boundary layer, the Reynolds shear stress is by far the most important stress component. Hence, the

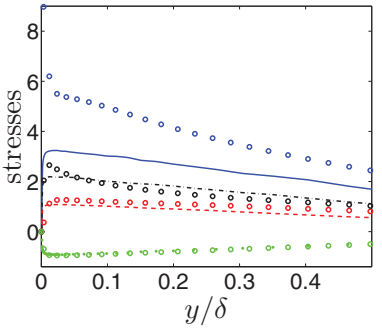

(a) Channel flow. Markers: DNS at $Re_\tau = 4\,200$ [27].

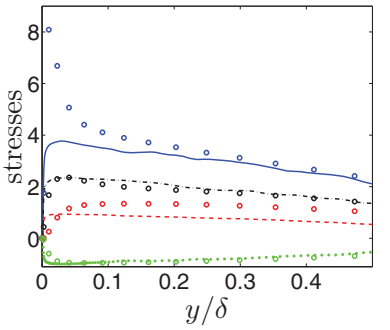

(b) Boundary-layer flow. Markers: DNS at $Re_\theta = 8\,300$ [28]

Figure 3. Added synthetic Reynolds stresses at the inlet. Subscript s denotes synthetic. ——: $\langle u_s' u_s' \rangle^+$; – –: $\langle v_s' v_s' \rangle^+$; – · –: $\langle w_s' w_s' \rangle^+$; · · ·: $\langle u_s' v_s' \rangle^+$.

Reynolds stress tensor is taken at the location where the magnitude of the turbulent shear stress is largest.

(5) Finally, the synthetic fluctuations are scaled with $\left(|\overline{u'v'}|/|\overline{u'v'}|_{max}\right)^{1/2}_{RANS}$, which is taken from the 1D RANS simulation.

The only constant used when generating these synthetic simulations is the prescribed integral length scale. Arvidson et al. [15] further extended this method by taking the integral length scale from the 1D RANS simulations.

Figure 3 shows the added synthetic fluctuations. The fluctuations differ slightly between the channel flow, the boundary-layer flow and the backward-facing step flow because the Reynolds stress tensor from EARSM and the shear stress from the RANS solutions are slightly different. As can be seen in Figure 3, the synthetic fluctuations are added over the entire inlet, both in the URANS and LES regions.

Matlab files for generation of the anisotropic fluctuations can be found in [26].

6. Results

6.1. Channel flow

The Reynolds number for the channel flow is $Re_\tau = 8000$. A $256 \times 96 \times 32$ mesh is used with $\Delta x = 0.1$, $\Delta z = 0.05$; a geometric stretching of 15% is used in the y direction ($y_{max} = 2 = 2\delta$). The wall-adjacent cell centre is located at $y^+ \simeq 0.7$ and at the centre $\Delta y \simeq 0.19\delta$. The mean inlet velocity profile is taken from a fully developed simulation using the zonal $k - \omega$ hybrid RANS–LES model. The k and ω are taken from a 1D RANS solution using the PDH model. The wall-parallel RANS–LES interface is prescribed at a fixed gridline at $y^+ \simeq 500$.

Figure 4 presents the turbulent viscosities, the modelled turbulent kinetic energy, the friction velocity and the shear stresses for different extensions of the transition region, x_{tr}. Figure 4(a) shows that, the smaller x_{tr}, the more rapidly the turbulent viscosity is reduced. When $x_{tr}/\delta = 0.1$, the reduction takes place over one cell. In this case, the commutation

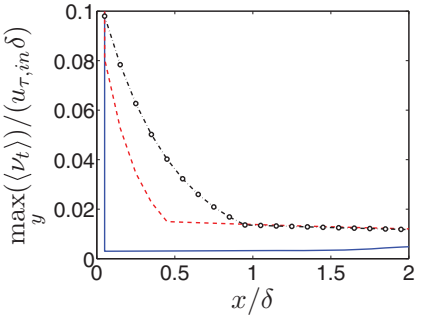

(a) Maximum turbulent viscosity in the LES region. Markers indicate location of cell centers.

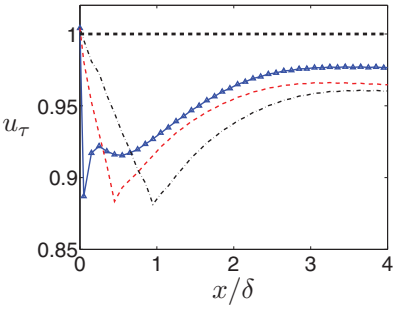

(b) Friction velocity. ▬ ▬: target value. Markers indicate location of cell centers.

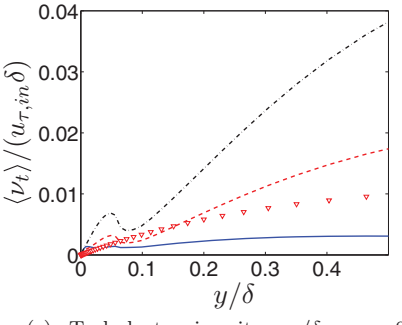

(c) Turbulent viscosity. $x/\delta = 0.25$. ▽: $\nu_t/10/(u_{\tau,in}\delta)$ at inlet (i.e. RANS).

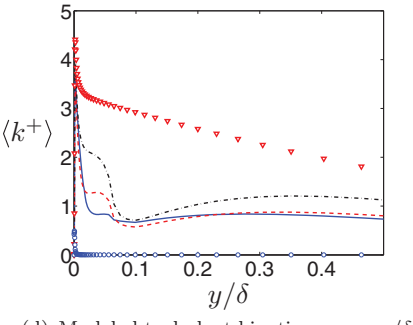

(d) Modeled turbulent kinetic energy. $x/\delta = 0.25$. ▽: $\langle k^+\rangle$ at inlet (i.e. RANS); ○: k_{LES} for $x_{tr}/\delta = 0.1$, see Eq. 11.

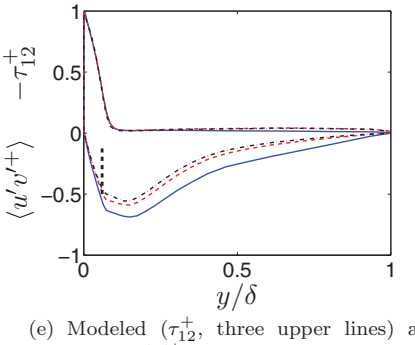

(e) Modeled (τ_{12}^+, three upper lines) and resolved ($\langle u'v'^+\rangle$, three lower lines) shear stress. $x/\delta = 0.25$.

Figure 4. Channel flow. ▬: $x_{tr}/\delta = 0.1$; ▬ ▬: $x_{tr}/\delta = 0.5$; ▬ · ▬: $x_{tr}/\delta = 1$.

term is simply $P^{k,c} = \bar{u}(k_{LES} - k_{RANS})/\Delta x \simeq -\bar{u}k_{RANS}/\Delta x$ (see Equation (11)) since k_{LES} is negligible(see Figure 4(d)) (this explains why it is unimportant where k_{LES} is evaluated, as mentioned below Equation (11)). Hence, the commutation term for $x_{tr}/\delta = 0.1$ corresponds to a convection term where k goes from its RANS (i.e. inlet) value to zero over one cell. The influence on the friction velocity (Figure 4(b)) is similar to that on the turbulent viscosities: the smaller the transition region, the earlier the minimum of u_τ is located. In fact, the minimum is located at the end of the transition region. As a consequence, the larger x_{tr}, the longer the distance it takes for u_τ to reach its fully developed

flow value (close to one). The reason why the fully developed value of u_τ is not one is that the synthetic fluctuations are not perfect: when inlet fluctuations are taken from a fully developed channel flow using the zonal $k-\omega$ hybrid RANS–LES model, the friction value does indeed quickly go to one (not shown). Figure 4(c–e) confirms the findings above, namely that, the shorter the transition region, the more quickly resolved turbulence is created and modelled turbulence is reduced. Figure 4(d) shows that the modelled turbulent kinetic energy is far from negligible in the LES region. However, it should be recalled that the turbulent kinetic energy does not enter the momentum equations (it is usually – as in the present work – included in the pressure). In channel and boundary-layer flow, the modelled turbulence influences the momentum equations via the shear stress. Hence, as noted in Davidson [29], it is the ratio of the modelled shear stress to the resolved shear stress that determines the effect of the modelled turbulence, not, as suggested by Pope [30], the ratio of modelled to total (i.e. modelled plus resolved) turbulent kinetic energy. The modelled and the resolved shear stresses are shown in Figure 4(e), and it can be seen that, as expected, the modelled shear stress in the LES region is negligible compared to the resolved shear stress.

Figure 5 shows the production and commutation term in the k equation close to the inlet. It can be seen that the magnitude of the commutation term is very large (Figure 5(a)), much larger than the production term, but it decreases with increasing transition length. It also decreases with x (see Figure 5(b)). The ratio of the commutation term to the production is shown in Figure 5(c), and it can be seen that it increases away from the wall and reaches approximately 600 at the centre (not shown). The reason that the ratio increases away from the wall is because the production term decreases (see Figure 5(a)). It may seem surprising that the k equation can accept such large sink terms without making the simulations unstable. The large sink terms are added *implicitly* on the left-hand side (i.e. to the diagonal element) of the discretised equation, which is very important. One way to reduce the large commutation term is, as mentioned above, to increase x_{tr}.

Above, $x_{tr}/\delta = 0.1$ was found to be the most efficient transition length for quickly creating resolved turbulence. Hence, below, we use $x_{tr}/\delta = 0.1$ to analyse the flow in more detail. Figure 6 shows that the velocities and the friction velocity are well predicted. It takes less than 3δ for the friction velocity (Figure 6(b)) to reach its fully developed value. Figure 6(c) shows that the turbulent viscosity is reduced from its inlet value (i.e. RANS) down to values corresponding to fully developed hybrid LES–RANS flow at already $x/\delta_{in} = 0.05$ (i.e. the cell layer adjacent to the inlet). Figure 6(d) presents the resolved turbulent streamwise fluctuations, and it can be seen that the resolved turbulence is quickly established although it takes a rather long distance to reach values close to fully developed hybrid LES–RANS.

Figure 6(e,f) shows the development of the peaks of resolved fluctuations and turbulent viscosity. It can be seen that the resolved fluctuations reach their fully developed peaks after approximately eight half-channel heights (the streamwise fluctuations develop much more slowly than the other two). The peak of the turbulent viscosity becomes fully developed at $x/\delta \simeq 3$.

In the plots shown so far, the commutation term in Equation (11) is also used in the URANS regions near the wall, although it includes k_{LES}, which may not be relevant in the URANS regions. Figure 7 shows the influence of different ways to compute the commutation term in the URANS regions. Three options are shown:

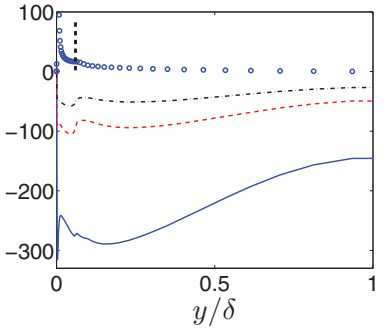

(a) $x/\delta = 0.05$. ○: Production term, P^k; ——: commutation term (Eq. 11), $x_{tr}/\delta = 0.1$; – – –: commutation term, $x_{tr}/\delta = 0.5$; –·–·–: commutation term, $x_{tr}/\delta = 1$.

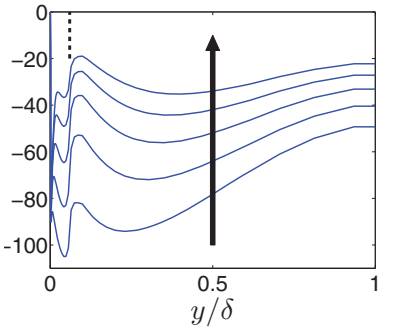

(b) Commutation term (Eq. 11) at different locations. $x_{tr}/\delta = 0.5$. $x/\delta = 0.05, \ldots 0.45$. The arrow indicates increasing x.

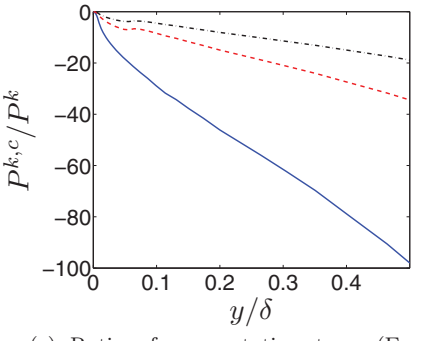

(c) Ratio of commutation term (Eq. 11) to production term, P^k. $x/\delta = 0.05$. ——: $x_{tr}/\delta = 0.1$; – – –: $x_{tr}/\delta = 0.5$; –·–·–: $x_{tr}/\delta = 1$.

Figure 5. Channel flow. Source terms in the *k* equation.

(1) the commutation term in Equation (11) is also used in the URANS region (this is the baseline option);
(2) no commutation term in the URANS region;
(3) the commutation term in the URANS region is computed according to Equation (12).

The turbulent viscosity close to the inlet (Figure 7(b)) shows that the baseline method strongly reduces ν_t as compared to when no commutation term is used. Equation (12) gives a turbulent viscosity in-between the two other methods, but Figure 7(a,c,d) shows that the influence of the different methods is small further downstream (at $x = 2.5\delta$).

Figure 8 shows the difference between the RANS length scale and viscosities (inlet) and the corresponding URANS quantities (close to the outlet). It can be seen that the RANS length scale and viscosity are more than twice and three times, respectively, the URANS length scale and viscosity. These differences are an argument for also using the commutation term in the URANS region, although – as was seen in Figure 7(a,c,d) – the influence is small. It may be noted that the turbulent viscosity in Figure 8(b) is approximately three

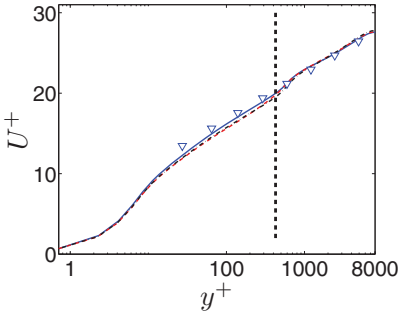

(a) Velocity. ——: inlet; – – –: $x = 2.5\delta$; –·–·–: $x = 24\delta$; ▽: $U^+ = \ln(y^+)/0.4 + 5.2$

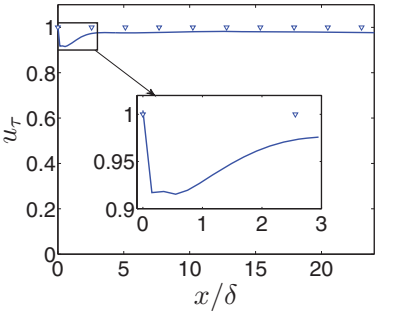

(b) Friction velocity. ▽: $u_\tau = 1$ (target value)

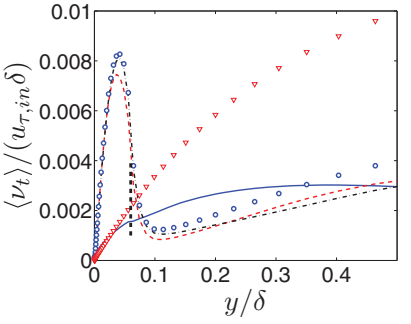

(c) Turbulent viscosity. ——: $x = 0.05\delta$; – – –: $x = 2.5\delta$; –·–·–: $x = 5.65\delta$; ▽: $\nu_t/(u_{\tau,in}\delta)/10$ at inlet (i.e. RANS).

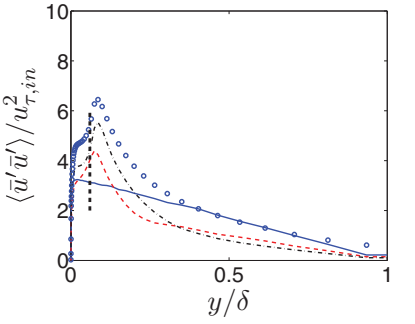

(d) Resolved turbulent stress. ——: $x/\delta = 0.05$; – – –: $x = 2.5\delta$; –·–·–: $x = 5.85\delta$.

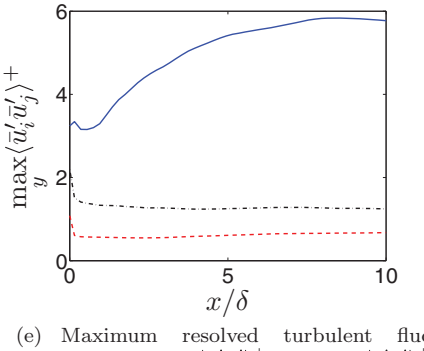

(e) Maximum resolved turbulent fluctuations. ——: $\langle \bar{u}'\bar{u}' \rangle^+$; – – –: $\langle v'v' \rangle^+$; –·–·–: $\langle w'w' \rangle^+$.

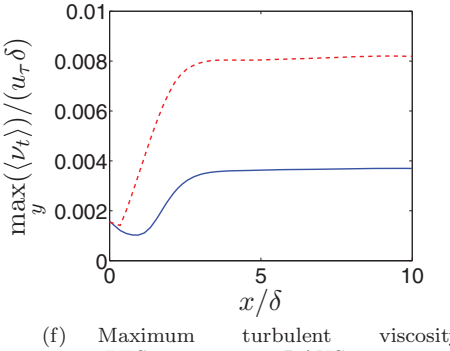

(f) Maximum turbulent viscosity. ——: LES region; – – –: RANS region.

Figure 6. Channel flow. : fully developed channel flow with the zonal hybrid RANS–LES model. The vertical thick dashed line indicates the RANS–LES interface.

times larger than in Figure 7(b). The reason is the strong reduction of the turbulent viscosity near the inlet; it increases in the URANS region further downstream(see Figure 6(f)).

As mentioned above, when $\Delta x_{tr} = 0.1$, the commutation term in the k equation corresponds to a negative convective term (see Equation (11)). Hence, it cancels the convective term at the inlet. Since the diffusion at the inlet is negligible, this means that we should be able to omit the commutation term in the k equation and instead use a homogeneous

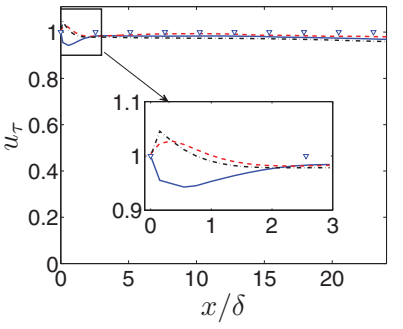

(a) Friction velocity. ▽: $u_\tau = 1$ (target value)

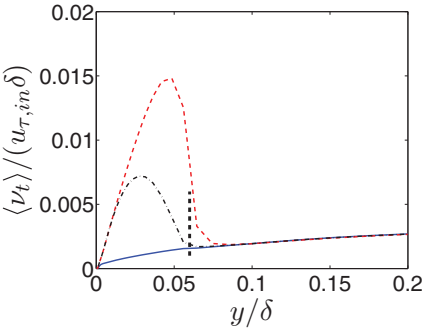

(b) Turbulent viscosity. $x = 0.05\delta$

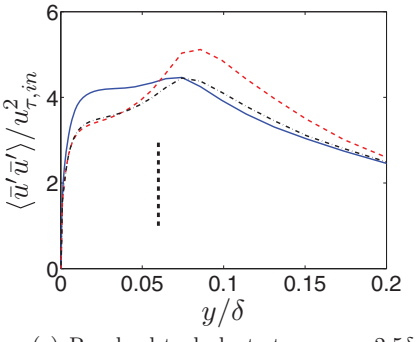

(c) Resolved turbulent stress. $x = 2.5\delta$

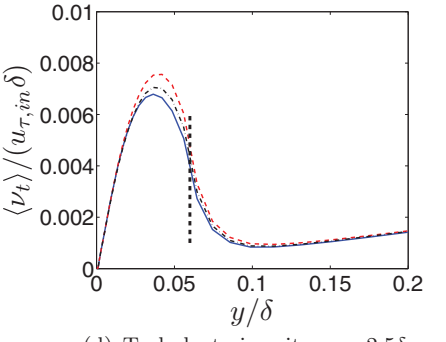

(d) Turbulent viscosity. $x = 2.5\delta$

Figure 7. Channel flow. The vertical thick dashed lines indicates the RANS–LES interface. ——: commutation terms in the URANS regions using Equation (11) (baseline); – –: no commutation terms in the URANS regions; – · –: commutation terms in the URANS regions using Equation (12).

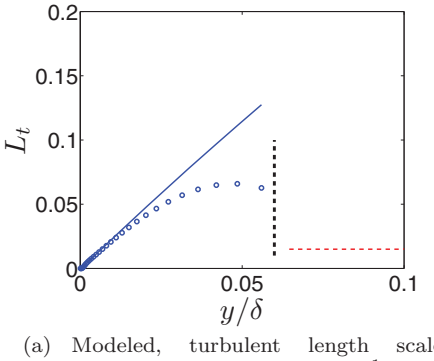

(a) Modeled, turbulent length scales. URANS and RANS: $L_t = C_k^{-1} k^{1/2}/\omega$. – –, LES: $L_t = \Delta_{dw}$ (Eq. 3).

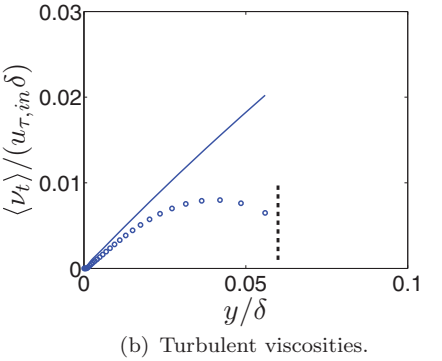

(b) Turbulent viscosities.

Figure 8. Channel flow. Length scale and viscosities. Vertical dashed line indicates the RANS–LES interface. ——: RANS (inlet values); ○: URANS ($x = 26\delta$).

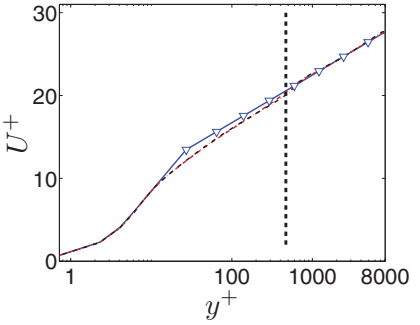

(a) Velocity. ——: inlet; – – –: $x = 2.5\delta$; –·–·–: $x = 24\delta$; ▽: $U^+ = \ln(y^+)/0.4 + 5.2$

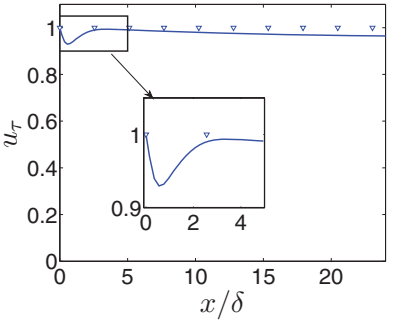

(b) Friction velocity. ▽: $u_\tau = 1$ (target value)

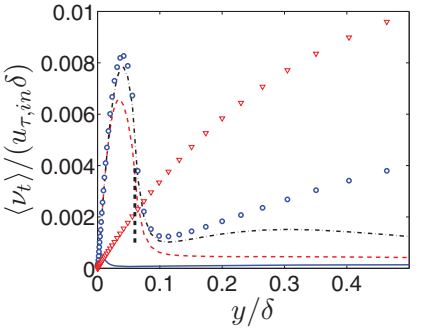

(c) Turbulent viscosity. ——: $x = 0.05\delta$; – – –: $x = 2.5\delta$; –·–·–: $x = 5.65\delta$; ▽: $\nu_t/(u_{\tau,in}\delta)/10$ at inlet (i.e. RANS).

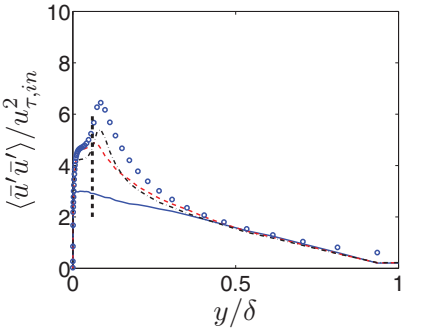

(d) Resolved turbulent stress. ——: $x/\delta = 0.05$; – – –: $x = 2.5\delta$; –·–·–: $x = 5.85\delta$.

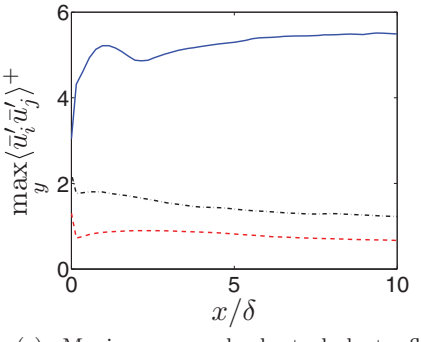

(e) Maximum resolved turbulent fluctuations. ——: $\langle \bar{u}'\bar{u}' \rangle^+$; – – –: $\langle v'v' \rangle^+$; –·–·–: $\langle w'w' \rangle^+$.

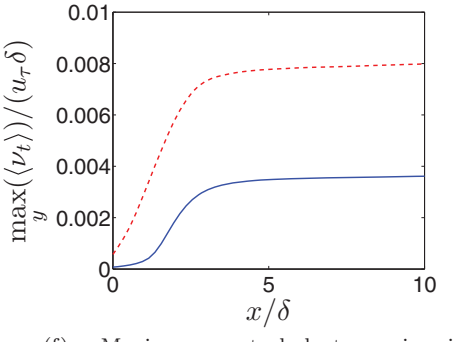

(f) Maximum turbulent viscosity. ——: LES region; – – –: RANS region.

Figure 9. Channel flow. No commutation term in the *k* equation. Homogeneous Neumann inlet boundary condition for *k*. : fully developed channel flow with the zonal hybrid RANS–LES model. The vertical thick dashed line indicates the RANS–LES interface.

Neumann inlet boundary condition. Figure 9 presents the velocity, the skin friction, the turbulent viscosity and the normal resolved stresses, where we use a homogeneous Neumann inlet condition for k and omit the commutation term in the k equation. We keep the commutation term (Equation (10)) in the ω equation. It can be seen that the skin friction (Figure 9(b)) reaches the target of one even faster than in Figure 6(b). The reason is that the

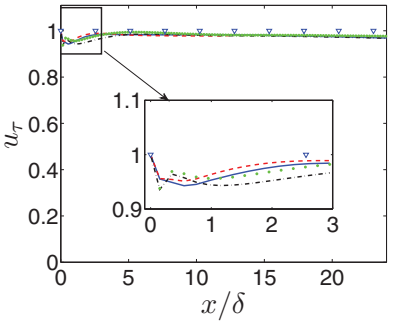

(a) Friction velocity. ▽: $u_\tau = 1$ (target value)

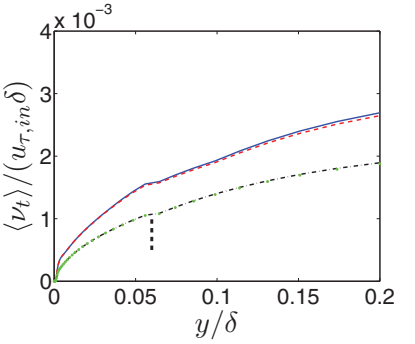

(b) Turbulent viscosity. $x = 0.05\delta$

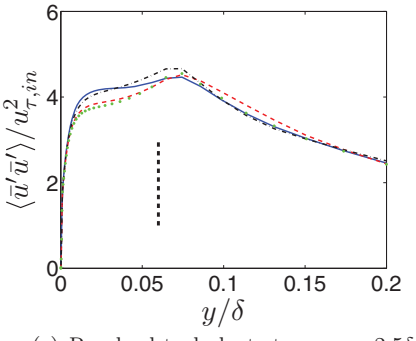

(c) Resolved turbulent stress. $x = 2.5\delta$

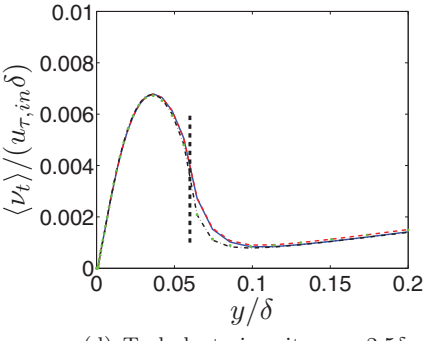

(d) Turbulent viscosity. $x = 2.5\delta$

Figure 10. Channel flow. The vertical thick dashed lines indicates the RANS–LES interface. ——: $\Delta x = 0.1$, $\Delta z = 0.05$ (baseline resolution); – –: $\Delta x = 0.1$, $\Delta z = 0.025$; – · –: $\Delta x = 0.05$, $\Delta z = 0.05$; · · ·: $\Delta x = 0.05$, $\Delta z = 0.025$.

turbulent viscosity is reduced more in Figure 9(c,f) than in Figure 6(c,f), which gives larger resolved stresses in Figure 9(d,e) than in Figure 6(d,e). The main reason why the differences are so large is probably that the discretised commutation terms do not exactly correspond to the convection term since the RANS turbulent kinetic energy in Equation (11) is taken at x and not at the inlet (i.e. $k_{RANS,\,x}$ (see Equation (11)) is used instead of k_{RANS}).

The baseline resolution in the wall-parallel plane is $\Delta x/\delta = 0.1$ and $\Delta z/\delta = 0.05$. Figure 10 shows how the results are influenced when the resolution is increased by a factor of two. It can be seen that influence is very small except close to the inlet. The turbulent viscosity close to the inlet (Figure 10(b)) is reduced when Δx is reduced, because the commutation term increases owing to a stronger streamwise derivative. It may be noted that the turbulent viscosity in Figure 10(d) is independent of the grid resolution. The reason is that it is computed as $C_{dw}d_w$ (see Equation (3)) for $y < 0.35\delta$.

6.2. Boundary-layer flow

For the developing boundary-layer flow, the Reynolds number is $Re_\theta = 11,000$ ($Re_{\tau,\,in} = 3\,400$). A $128 \times 192 \times 32$ mesh is used with $\Delta x = 0.1$, $\Delta z = 0.05$; a geometric stretching of less than 15% is used in the boundary layer in the y direction. The inlet boundary-layer thickness ($\delta_{in} = 0.8$) is covered by approximately 110 cells. The wall-adjacent cell centre is

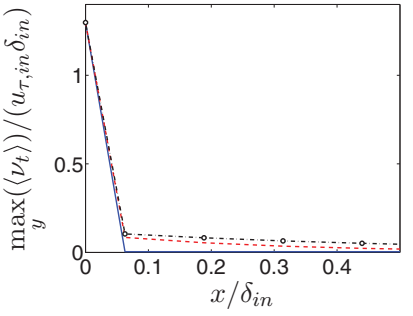

(a) Maximum turbulent viscosity in the LES region. Markers denote location of cell centers.

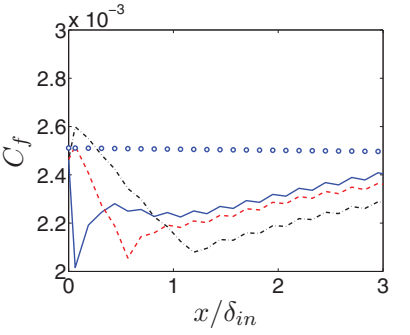

(b) Skin friction. ○: target value. Markers indicate location of cell centers.

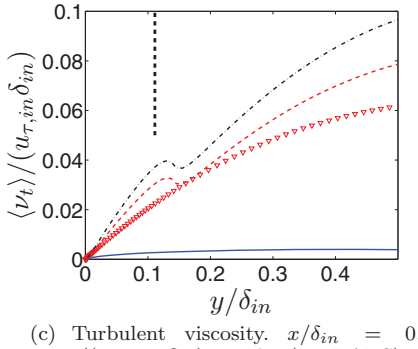

(c) Turbulent viscosity. $x/\delta_{in} = 0.06$. ▽: $\nu_t/(20u_{\tau,in}\delta_{in})$ at inlet (i.e. RANS).

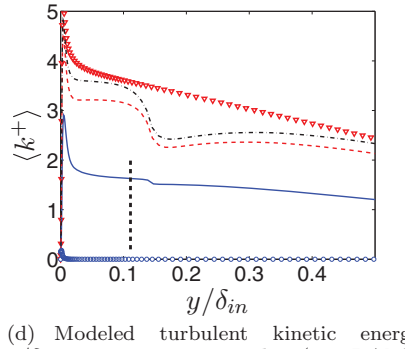

(d) Modeled turbulent kinetic energy. $x/\delta_{in} = 0.06$. ▽: at inlet (i.e. RANS); ○: k_{LES} for $x_{tr}/\delta_{in} = 0.1$, see Eq. 11.

Figure 11. Boundary-layer flow. ——: $x_{tr}/\delta_{in} = 0.125$; – –: $x_{tr}/\delta_{in} = 0.25$; – · –: $x_{tr}/\delta_{in} = 0.375$; : at inlet (i.e. RANS). The vertical thick dashed line indicates the RANS–LES interface.

located at $y^+ \simeq 0.35$ and, at the edge of the boundary-layer, $\Delta y \simeq 0.013\delta$. The mean inlet velocity profile is taken from the linear and the log-law, which are connected with another log law in the buffer layer

$$U_{in}^+ = \begin{cases} y^+ & y^+ \le 5 \\ -2.23 + 4.49\ln(y^+) & 5 < y^+ < 30 \\ \frac{1}{\kappa}\ln(y^+) + B + \frac{2\Pi}{\kappa}\sin^2\left(\frac{\pi y}{2\delta}\right) & y^+ \ge 30 \end{cases}, \tag{13}$$

where $\kappa = 0.38$, $B = 4.1$ and $\Pi = 0.5$ [31,32]. The k and ω are taken from a RANS solution using the PDH model. The reason why the velocity is not taken from a RANS simulation is that the RANS predictions do not give a proper relation between the skin friction and the momentum thickness (e.g. $C_f = 0.03Re_\theta^{-0.268}$ [33, Equations (7–79)]). The influence is shown in Figure 13(b). The wall-parallel RANS–LES interface is prescribed at a fixed gridline at $y^+ \simeq 500$.

Figure 11 presents the sensitivity to the transition length of the boundary-layer flow. Note that the predictions of this flow in [34] are very different due to an incorrect inlet boundary condition on ω. Similar to the channel flow (Figure 4(a)), the turbulent viscosity

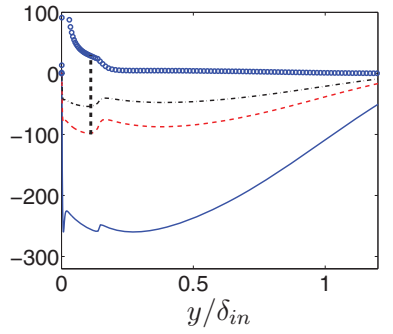

(a) $x/\delta_{in} = 0.06$. ○: Production term, $x_{tr}/\delta_{in} = 0.125$; ——: commutation term (Eq. 11), $x_{tr}/\delta_{in} = 0.125$; – – : commutation term, $x_{tr}/\delta_{in} = 0.25$; –·– : commutation term, $x_{tr}/\delta_{in} = 0.375$.

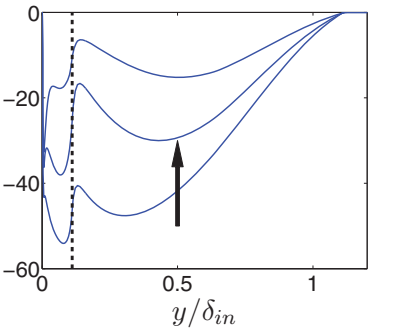

(b) Commutation term (Eq. 11). $x_{tr}/\delta_{in} = 0.375$. $x/\delta_{in} = 0.06, 0.18, 0.31$. The arrow indicates increasing x.

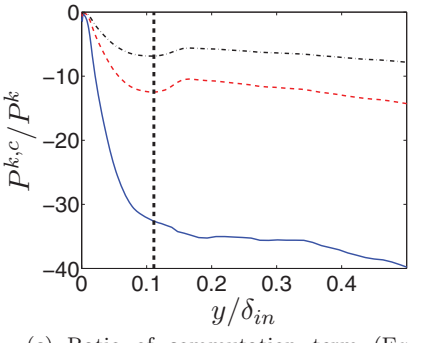

(c) Ratio of commutation term (Eq. 11) to production term, P^k. $x/\delta_{in} = 0.06$. ——: $x_{tr}/\delta = 0.125$; – – : $x_{tr}/\delta = 0.25$; –·– : $x_{tr}/\delta = 0.375$.

Figure 12. Boundary-layer flow. Source terms in the k equation (scaled with $u^3_{\tau,in}/\delta_{in}$).

is strongly reduced near the inlet. The skin friction in Figure 11(b) is well predicted and, as is the case for the channel flow, it approaches its target value faster, the shorter the transition length. An accurate value is obtained within three boundary-layer thicknesses. The turbulent viscosity profiles in Figure 11(c) show that the turbulent viscosity is strongly reduced at the cells adjacent to the inlet; the reduction factor for $x_{tr}/\delta_{in} = 0.125$ at, for example, $y/\delta_{in} = 0.4$ is 290 compared to the inlet value. It can be noted that the modelled turbulent kinetic energy, k (Figure 11(d)), is reduced much less than the turbulent viscosity (as for the channel flow, see Figure 4(c,d)). The reason is, of course, that ω is increased (not shown). Figure 11(d) also includes k_{LES} which is used in the commutation term (see Equation (11)) which, as in the channel flow (cf. Figure 4(d)), is negligible compared to k_{RANS}.

Figure 12 presents the production and commutation terms in the k equation. As in the channel flow, the commutation term is much larger than the production term (Figure 12(a)) and it is as large as in the channel flow. The streamwise gradient of the commutation term (see Figure 12(b)) is also as large as in the channel flow (cf. Figure 5(b)). Figure 12(c) shows the ratio, and as in the channel flow (Figure 5(c)), it increases away from the wall; the ratio

is smaller than in channel flow. At the edge ($y = \delta$), the ratio reaches approximately 100 (not shown).

Since the short transition length works well, some detailed comparisons are presented below for $x_{tr}/\delta_{in} = 0.125$. Figure 13 shows that, for $x_{tr}/\delta_{in} = 0.125$, the flow reaches fully developed conditions fairly rapidly: after approximately $5\delta_{in}$, the skin friction (Figure 13(b)), the turbulent viscosities (Figure 13(c,f)) and the resolved turbulence (Figure 13(d,e)) have reached their fully developed values. Contrary to the channel flow, where the streamwise fluctuations increase much more slowly than the other two normal Reynolds stresses, here all three normal Reynolds stresses quickly reach their fully developed peak values. The streamwise resolved fluctuations agree fairly well with DNS data at already $x_{tr}/\delta_{in} = 0.06$ (Figure 13(d)), and the turbulent viscosity is reduced at the RANS–LES interface from the RANS (inlet) value by a factor of 180 (Figure 13(c)). The mean inlet velocity is taken from the log-law (see Equation (13)). Figure 13(b) shows the skin friction when instead the mean inlet velocity is taken from a 2D RANS simulation using the PDH model [24].

6.3. Backward-facing step flow

The Reynolds number for the backward-facing step flow is $Re_H = 28,000$. The experiments were made by Vogel and Eaton [35]. The grid has $336 \times 152 \times 64$ cells. x, y, z denote the streamwise (x), wall-normal (y) and spanwise (z) directions, respectively (see Figure 14). The step is covered by 96×52 cells in x and y. The inlet boundary layers at the upper wall and the step are covered by 45 cells (the boundary-layer width is one step height, H); the grid is stretched by 1.12 in the lower and upper boundary layers. The grid above the step is symmetric around $y/H = 3$. A constant grid spacing is used in the x direction in $-4.6 < x/H < -0.27$ with $\Delta x \simeq 0.05$; the grid is geometrically compressed by 0.89 in the region $-0.27 < x/H < 0$. The extent of the domain in the spanwise direction is 1.6. The mesh in the recirculation region is taken from [16].

The inlet mean profile is taken from a RANS simulation of a 2D simulation using the AKN model [36]. For the temperature, the inlet profile is $\bar{t} = 0$ (constant in both space and time). At the lower wall, at $y = 0$, a constant heat flux, q_w, is used for $x > 0$. The inlet bulk velocity and H are set to one, so that $\nu = 1/Re_H$. Contrary to the channel flow and the boundary-layer flow, the Reynolds number for this flow is rather low and hence the boundary layers are treated in LES mode.

Embedded LES is used for this flow. This means that RANS is used up to a location close to the step – the RANS–LES interface, x_{R-L}. At this location, the length scale, ℓ_t, in the dissipation term of the k equation (Equation (1)) is switched from RANS to LES and the commutation terms are added so that the flow switches from RANS to LES mode. As an option, synthetic fluctuations are added at the step. However, it was found that it is not stable to add the fluctuations at the step, so the synthetic fluctuations (and the commutation terms) are added upstream of the step, at $x/H = -1$. We have run six cases for the backward-facing step flow.

(1) no commutation term, no synthetic fluctuations, $x_{R-L} = 0$;
(2) commutation term, no synthetic fluctuations, $x_{R-L} = 0$;

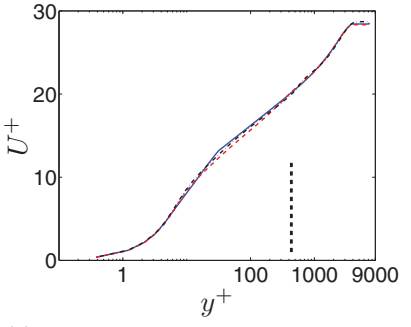

(a) Velocity. ——: inlet; – –: $x = 2.35\delta_{in}$; –·–: $x = 5.95\delta_{in}$.

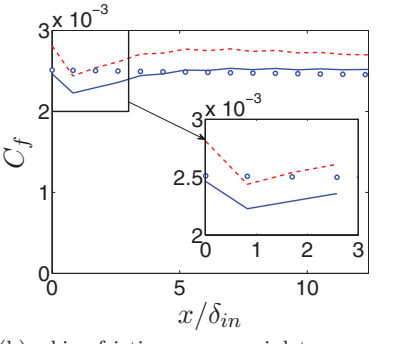

(b) skin friction. ——: inlet mean velocity profile from Eq. 13; – –: inlet mean velocity profile from PDH model; ○: $0.37\,(log_{10}Re_x)^{-2.584}$.

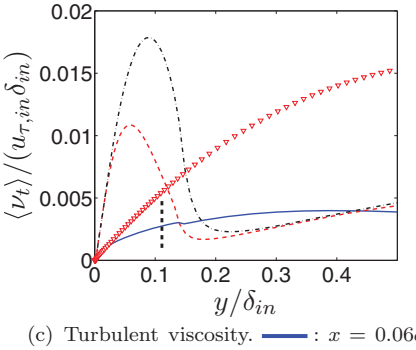

(c) Turbulent viscosity. ——: $x = 0.06\delta_{in}$; – –: $x = 2.35\delta_{in}$; –·–: $x = 11.9\delta_{in}$; ▽: $\nu_t/(u_{\tau,in}\delta_{in})/80$ at inlet (i.e. RANS)

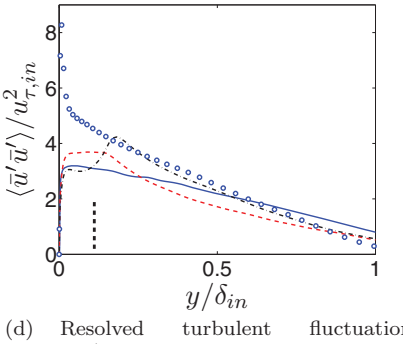

(d) Resolved turbulent fluctuations. ——: $x/\delta_{in} = 0.06$; – –: $x = 2.35\delta_{in}$; –·–: $x = 11.9\delta_{in}$; ○: DNS at $Re_\theta = 8\,300$ [28].

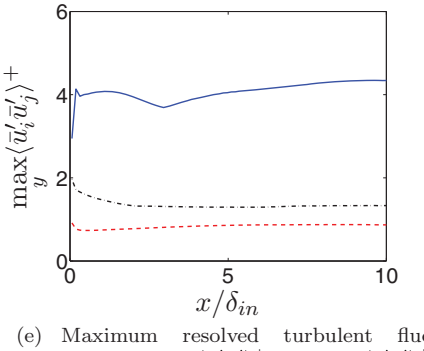

(e) Maximum resolved turbulent fluctuations. ——: $\langle \bar{u}'\bar{u}' \rangle^+$; – –: $\langle v'v' \rangle^+$; –·–: $\langle w'w' \rangle^+$.

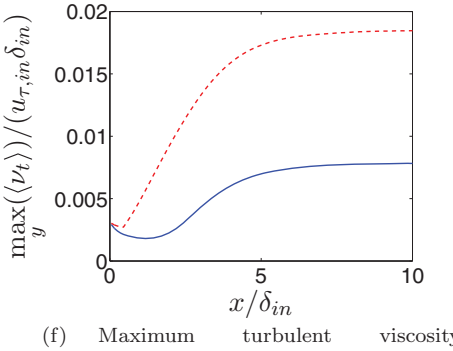

(f) Maximum turbulent viscosity. ——: LES region; – –: RANS region.

Figure 13. Boundary-layer flow. $x_{tr}/\delta_{in} = 0.125$. The vertical thick dashed line indicates the RANS–LES interface.

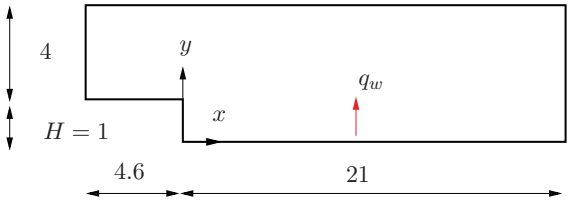

Figure 14. Backward-facing step flow.

(3) no commutation term, synthetic fluctuations at the RANS–LES interface (see Equation (14)), $x_{R-L} = -H$;
(4) commutation term, synthetic fluctuations at the RANS–LES interface (see Equation (14)), $x_{R-L} = -H$;
(5) no commutation term, no synthetic fluctuations, $x_{R-L} = -H$;
(6) commutation term, no synthetic fluctuations, $x_{R-L} = -H$.

In the channel flow and boundary-layer flow, the synthetic fluctuations are prescribed as inlet boundary conditions. In the backward-facing flow, we carry out embedded LES (i.e. RANS upstream of x_{R-L} and LES downstream) and hence the synthetic fluctuations are added as additional source terms in the momentum and continuity equations. For the $\bar{v}$ equation, for example, the sources read

$$\begin{aligned} S_U &= C\Delta y\Delta z, \\ a_P &= u_s'\Delta y\Delta z, \\ C &= \bar{u}_u v_s' + \bar{v}_u u_s' + u_s' v_s', \end{aligned} \tag{14}$$

where subscripts u and s indicate the cell upstream of the interface and synthetic fluctuation, respectively. S_U and a_P are the source term and the diagonal element in the matrix for the discretised $\bar{u}$ momentum equation, respectively. The synthetic fluctuations, $u_{s,i}'$, are generated in exactly the same way as the inlet fluctuation for the channel flow and boundary-layer flow simulations (see Section 5).

Figures 15–18 present the skin friction, the Stanton number ($St = Nu/(Re_H Pr)$), the streamwise mean velocity, streamwise resolved fluctuations and turbulent viscosities for Cases 1–4. First, it may be noted that the commutation terms improve the Stanton number when no synthetic fluctuations are added (Figure 16(a)), but they have little influence on the skin friction (Figure 15). The velocity profiles (Figure 17) show that the synthetic fluctuations give a slightly stronger recirculation, which can also be seen in the skin friction. The commutation terms have no visible effect on the mean flow. However, the commutation terms have a strong effect on the turbulent viscosity (Figures 18(a,b)) while the effect is much smaller for the resolved fluctuations (Figures 18(c,d)). The commutation terms do increase the resolved turbulence in the shear layer, but not by a great deal. The reason for the small influence on the mean flow and on the resolved turbulence is that the flow itself generates large resolved turbulent fluctuations at the step ($x = 0$) so that the effect of the strongly reduced turbulent viscosity is almost negligible. Looking at the resolved fluctuations (Figure 18(c)), it can be seen that adding synthetic fluctuations gives *smaller* values than when no synthetic fluctuations are added. This may seem surprising. The reason is

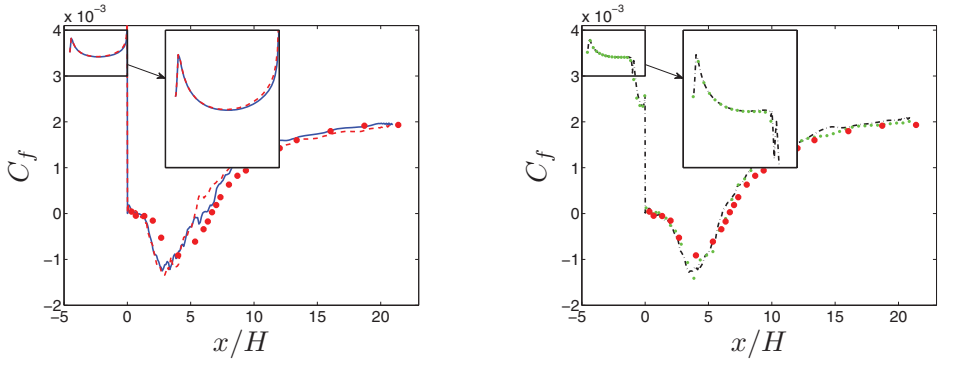

(a) No synthetic fluctuations. $x_{R-L}/H = 0$. —— no commutation term (Case 1); – – commutation term (Case 2).

(b) Synthetic fluctuations at $x_{R-L}/H = -1$. –·– no commutation term (Case 3); ··· commutation term (Case 4).

Figure 15. Backward-facing step flow. Skin friction. Markers: experiments [35].

that, in the case with synthetic fluctuations (Cases 3 and 4), the RANS–LES interface is located at $x = -H$, whereas, when no synthetic fluctuations are used (Cases 1 and 2), it is located at $x = 0$. The result is that, with synthetic fluctuations, the shear $(\partial\bar{u}/\partial y)$ in the initial shear layer at $x = 0$ is much smaller than without synthetic fluctuations, because the skin friction on the step (i.e. $x \leq 0$) is much smaller (see Figure 15). The maximum shear in the initial shear layer is equal to the maximum velocity gradient, which is directly proportional to the skin friction. The skin friction is smaller with synthetic fluctuations because the synthetic fluctuations do not manage to force the equations to switch from RANS mode to full LES mode from $x = -H$ to $x = 0$ (note that a correct, large skin friction would be obtained if the RANS–LES interface were located further upstream, as in [37], where the synthetic fluctuations are used as inlet boundary conditions at $x = -4.7H$). A large shear in the initial shear layer generates large resolved fluctuations, which explains the results in Figure 18(c).

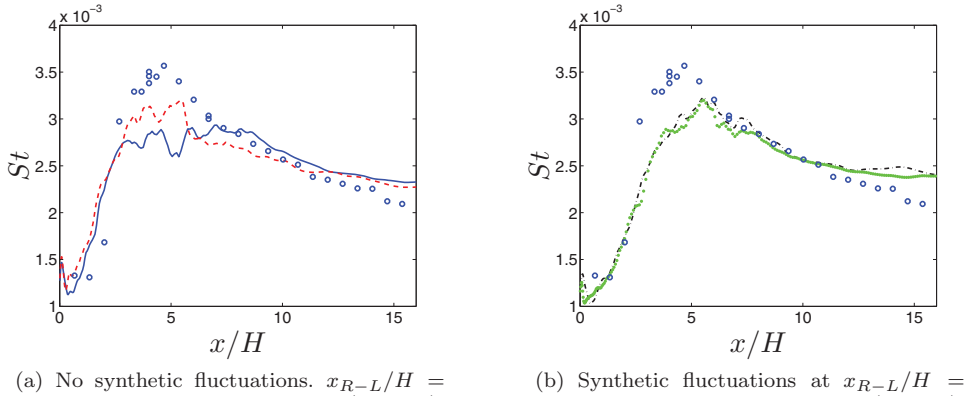

(a) No synthetic fluctuations. $x_{R-L}/H = 0$. —— no commutation term (Case 1); – – commutation term (Case 1).

(b) Synthetic fluctuations at $x_{R-L}/H = -1$. –·– no commutation term (Case 3); ··· commutation term (Case 4).

Figure 16. Backward-facing step flow. Stanton number. Markers: experiments [35].

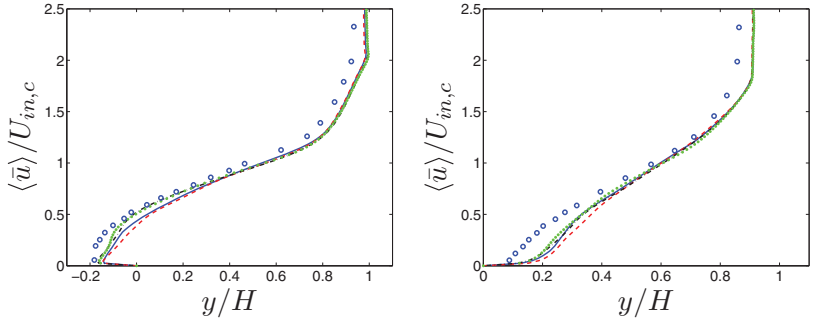

(a) $x = 3.2H$. (b) $x = 7.2H$.

Figure 17. Backward-facing step flow. Mean velocity profiles. ——— : no commutation term, no synthetic fluctuations (Case 1); – – : commutation term, no synthetic fluctuations (Case 2); – · – : no commutation term, synthetic fluctuations (Case 3); . . . : commutation term, synthetic fluctuations (Case 4). Markers: experiments [35].

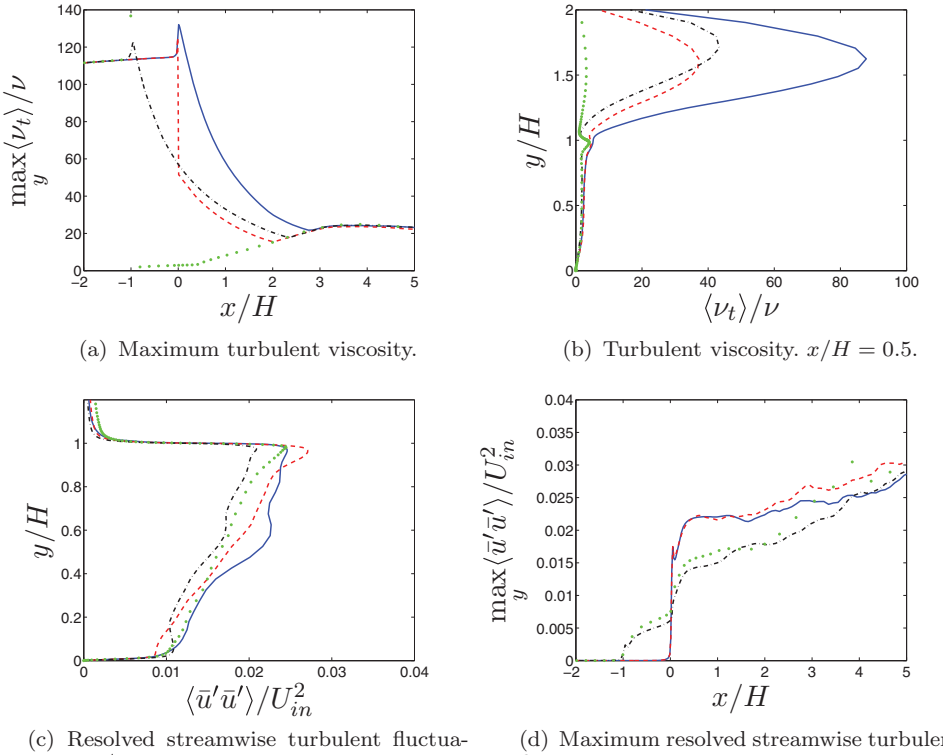

(a) Maximum turbulent viscosity. (b) Turbulent viscosity. $x/H = 0.5$.

(c) Resolved streamwise turbulent fluctuations. $x/H = 3$. (d) Maximum resolved streamwise turbulent fluctuations.

Figure 18. Backward-facing step flow. ——— : no commutation term, no synthetic fluctuations (Case 1); – – : commutation term, no synthetic fluctuations (Case 2); – · – : no commutation term, synthetic fluctuations (Case 3); . . . : commutation term, synthetic fluctuations (Case 4).

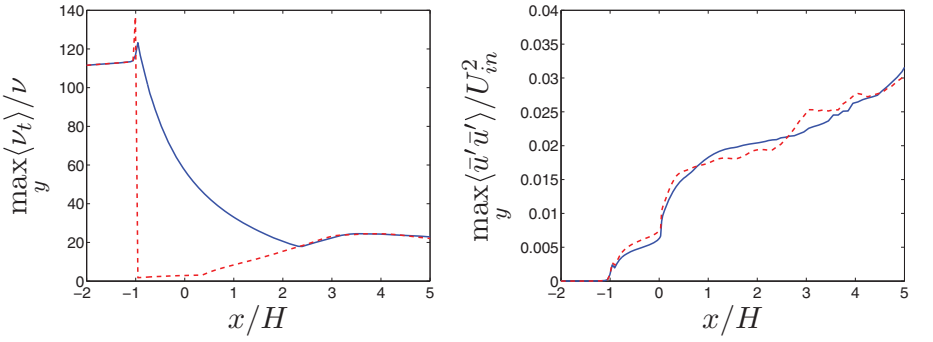

(a) Maximum turbulent viscosity.

(b) Maximum resolved turbulent fluctuations.

Figure 19. Backward-facing step flow. RANS–LES interface at $x = -H$. No synthetic fluctuations. ——— : no commutation term (Case 5); – – : commutation term (Case 6).

Figure 19 shows the results when the RANS–LES interface is located at $x = -H$ and no synthetic fluctuations are added (Cases 5 and 6). As expected, the resolved fluctuations are much smaller than when the interface is located at the step (i.e. $xR{-}L = 0$) (Cases 1 and 2) (see Figure 18(d)), because the skin friction (and thus the shear in the initial shear layer) is much smaller.

The main lesson for this test case is that the commutation terms perform as expected, i.e. they strongly reduce the turbulent viscosity, but that they are not important in increasing the resolved turbulence; this is taken care of by the flow itself through the large shear. What is important is to make sure that the predicted skin friction at the step ($x = 0$) is correct (i.e. sufficiently large) because it determines the maximum shear in the initial shear layer, which rapidly creates resolved turbulence in the shear layer and thereby quickly switches the flow from RANS to LES mode.

7. Concluding remarks

A novel method of treating k and ω at the inlet has been presented and evaluated in channel flow, boundary-layer flow and backstep-facing flow. A commutation term is added in the region near the inlet – or, in embedded LES, at the RANS–LES interface – in the k and ω equations. The commutation terms are added either only in the cell layer adjacent to the inlet or in a transition region; it is found that the former choice is best. For this case, this term corresponds to a negative convection term in the k equation. This suggests, provided that the diffusion at the inlet is negligible, that the commutation term can be omitted and that a homogeneous Neumann boundary condition can be used at the inlet (keeping the commutation term in the ω equation). It is found that this option gives very good results.

The proposed method includes no tuning constants. The synthetic fluctuations include one input parameter, however, namely the integral length scale. In Arvidson et al. [15], the present method is used for embedded channel flow and, in that work, the integral length scale is taken from the RANS simulation.

The commutation terms have a large effect for the channel flow and the boundary-layer flow, where they strongly reduce the turbulent viscosity and thereby promote the transition

to fully resolved LES mode. For the backward-facing step flow, it is found that the commutation terms do reduce the turbulent viscosity but that they are not important in creating turbulence in the shear layer. They are beneficial, but the effect is small. The reason is that the shear layer is highly unstable in itself. It is found that it is much more important to predict a large, correct skin friction at the step. This ensures that the shear in the initial shear layer is large, which generates large resolved turbulence fluctuations.

Disclosure statement

No potential conflict of interest was reported by the author.

References

[1] Travin A, Shur M, Strelets M, et al. Detached-eddy simulations past a circular cylinder. Flow Turbul Combust. 2000;63:293–313.
[2] Chauvet N, Deck S, Jacquin L. Zonal detached eddy simulation of a controlled propulsive jet. AIAA J. 2007;45(10):2458–2473.
[3] Deck S. Recent improvements in the zonal detached eddy simulation (ZDES) formulation. Theor Comput Fluid Dyn. 2012;26(6):523–550.
[4] Kok J, van der Ven H. Capturing free shear layers in hybrid RANS-LES simulations of separated flow. Stockholm: National Aerospace Laboratory (NLR); 2012. (NLR-TP-2012-333).
[5] Mockett C, Fuchs M, Garbaruk A, et al. Two non-zonal approaches to accelerate RANS to LES transition of free shear layers in DES. In: Girimaji S, Haase W, Peng SH, Schwamborn D, editors. Progress in hybrid rans-les modelling. Vol. 130, Notes on numerical fluid mechanics and multidisciplinary design. Berlin: Springer; 2014. p. 187–201.
[6] Nicoud F, Ducros F. Subgrid-scale stress modelling based on the square of the velocity gradient tensor. Flow Turbul Combust. 1999;62(3):183–200.
[7] Nicoud F, Toda HB, Cabrit O, et al. Using singular values to build a subgrid-scale model for large eddy simulations. Phys Fluids. 2011;23(8):085106. Available from: http://scitation.aip.org/content/aip/journal/pof2/23/8/10.1063/1.3623274
[8] Shur M, Spalart P, Strelets M, et al. An enhanced version of DES with rapid transition from RANS to LES in separated flows. Flow Turbul Combust. 2015;95:709–737.
[9] Girimaji SS, Wallin S. Closure modeling in bridging regions of variable-resolution (VR) turbulence computations. J Turbul. 2013;14(1):72–98.
[10] Davidson L. Zonal PANS: evaluation of different treatments of the RANS-LES interface. J Turbul. 2016;17(3):274–307.
[11] Davidson L. Hybrid LES-RANS: back scatter from a scale-similarity model used as forcing. Phil Trans Royal Soc A. 2009;367(1899):2905–2915.
[12] Bardina J, Ferziger JH, Reynolds WC. Improved subgrid scale models for large eddy simulation. AIAA 80-1357; Snomass, CO; 1980.
[13] Peng SH. Hybrid RANS-LES modelling with an energy backscatter function incorporated in the LES mode. In: Turbulence, Heat and Mass Transfer, THMT-12; Palermo, Sicily/Italy; 2012.
[14] Hamba F. Analysis of filtered Navier–Stokes equation for hybrid RANS/LES simulation. Phys Fluids A. 2011;23(015108).
[15] Arvidson S, Davidson L, Peng SH. Hybrid RANS-LES modeling based on a low-Reynolds-number $k - \omega$ model. AIAA J. 2016;54(12):4032–4037.
[16] Shur ML, Spalart PR, Strelets MK, et al. A hybrid RANS-LES approach with delayed-DES and wall-modelled LES capabilities. Int J Heat Fluid Flow. 2008;29:1638–1649.
[17] Ghosal S, Moin P. The basic equations for the large eddy simulation of turbulent flows in complex geometry. J Comp Phys. 1995;118:24–37.
[18] Chaouat B, Schiestel R. Partially integrated transport modeling method for turbulence simulation with variable filters. Phys Fluids. 2013;25(125102).

[19] Davidson L. The PANS $k-\varepsilon$ model in a zonal hybrid RANS-LES formulation. Int J Heat Fluid Flow. 2014;46:112–126.
[20] Davidson L, Peng SH. Hybrid LES-RANS: a one-equation SGS model combined with a $k-\omega$ model for predicting recirculating flows. Int J Numer Methods Fluids. 2003;43:1003–1018.
[21] Emvin P. The full multigrid method applied to turbulent flow in ventilated enclosures using structured and unstructured grids [Ph.D. thesis]. Göteborg: Department of Thermo and Fluid Dynamics, Chalmers University of Technology; 1997.
[22] Davidson L. Using isotropic synthetic fluctuations as inlet boundary conditions for unsteady simulations. Adv Appl Fluid Mech. 2007;1(1):1–35.
[23] Davidson L, Peng SH. Embedded large-eddy simulation using the partially averaged Navier–Stokes model. AIAA J. 2013;51(5):1066–1079.
[24] Peng SH, Davidson L, Holmberg S. A modified low-Reynolds-number $k-\omega$ model for recirculating flows. J Fluids Eng. 1997;119:867–875.
[25] Wallin S, Johansson AV. A new explicit algebraic Reynolds stress model for incompressible and compressible turbulent flows. J Fluid Mech. 2000;403:89–132.
[26] Davidson L. Available from: http://www.tfd.chalmers.se/~lada/projects/inlet-boundary-conditions/proright.html
[27] Lozano-Duran A, Jimenez J. Effect of the computational domain on direct simulations of turbulent channels up to $Re_\tau = 4200$. Phys Fluids A. 2014;26(011702).
[28] Eitel-Amor G, Orlu R, Schlatter P. Simulation and validation of a spatially evolving turbulent boundary layers up to $Re_\theta = 8300$. Int J Heat Fluid Flow. 2014;47:57–69.
[29] Davidson L. Large eddy simulations: how to evaluate resolution. Int J Heat Fluid Flow. 2009;30(5):1016–1025.
[30] Pope S. Ten questions concerning the large-eddy simulations of turbulent flows. New J Phys. 2004;6(35):1–24.
[31] Österlund M, Johansson A, Nagib H, et al. A note on the overlap region in turbulent boundary layers. Phys Fluids A. 2000;12(1):1–4.
[32] Österlund J. Experimental studies of zero pressure-gradient turbulent boundary-layer flow [Ph.D. thesis]. Stockholm: Department of Mechanics, Royal Institute of Technology; 1999.
[33] Hinze JO. Turbulence. 2nd ed. New York: McGraw-Hill; 1975.
[34] Davidson L. *Two-equation hybrid RANS-LES models: a novel way to treat k and ω at the inlet*. In: Turbulence, Heat and Mass Transfer, THMT-15; Sarajevo, Bosnia and Herzegovina; 2015.
[35] Vogel JC, Eaton JK. Combined heat transfer and fluid dynamic measurements downstream a backward-facing step. J Heat Transfer. 1985;107:922–929.
[36] Abe K, Kondoh T, Nagano Y. A new turbulence model for predicting fluid flow and heat transfer in separating and reattaching flows – 1. Flow field calculations. Int J Heat Mass Transfer. 1994;37(1):139–151.
[37] Davidson L. Large eddy simulation of heat transfer in boundary layer and backstep flow using PANS. In: Turbulence, Heat and Mass Transfer, THMT-12; Palermo, Sicily/Italy; 2012. (Corrected version available from: http://www.tfd.chalmers.se/~lada/).